Virology 452-453 (2014) 133–142

Contents lists available at ScienceDirect

Virology

journal homepage: www.elsevier.com/locate/yviro

The p33 auxiliary replicase protein of Cucumber necrosis virus targets peroxisomes and infection induces *de novo* peroxisome formation from the endoplasmic reticulum

D'Ann Rochon [a,b,*], Bhavana Singh [b], Ron Reade [a], Jane Theilmann [a], Kankana Ghoshal [b], Syed Benazir Alam [b], Ajay Maghodia [a,b]

[a] Agriculture and Agri-Food Canada Pacific Agri-Food Research Centre, 4200 Hwy 97, Summerland, BC, Canada V0H 1Z0
[b] University of British Columbia Faculty of Land and Food Systems Vancouver, BC, Canada V6T 1Z4

ARTICLE INFO

Available online 31 January 2014

Keywords:
Tombusvirus
RNA virus
Peroxisomes
Spherules
De novo peroxisome formation
Necrosis
Endoplasmic reticulum

ABSTRACT

Tombusviruses replicate on pre-existing organelles such as peroxisomes or mitochondria, the membranes of which become extensively reorganized into multivesicular bodies (MVBs) during the infection process. *Cucumber necrosis virus* (CNV) has previously been shown to replicate in association with peroxisomes in yeast. We show that CNV induces MVBs from peroxisomes in infected plants and that GFP-tagged p33 auxiliary replicase protein colocalizes with YFP_{SKL}, a peroxisomal marker. Most remarkably, the ER of CNV infected *Nicotiana benthamiana* 16C plants undergoes a dramatic reorganization producing numerous new peroxisome-like structures that associate with CNV p33, thus likely serving as a new site for viral RNA replication. We also show that plants agroinfiltrated with p33 develop CNV-like necrotic symptoms which are associated with increased levels of peroxide. Since peroxisomes are a site for peroxide catabolism, and peroxide is known to induce plant defense responses, we suggest that dysfunctional peroxisomes contribute to CNV induced necrosis.

Introduction

Cucumber necrosis virus (CNV) is a member of the *Tombusvirus* genus in the Family *Tombusviridae*. The plus-strand, positive-sense RNA genome of CNV contains five open reading frames (ORFs) (Fig. 1) (Rochon and Tremaine, 1989). ORF1 encodes a 33 kDa auxiliary replicase protein (p33) and the readthrough of this ORF produces a 92 kDa protein containing RNA dependent RNA polymerase motifs. ORF3 encodes the 41 kDa coat protein which assembles with viral RNA to form virions with $T=3$ icosahedral symmetry (Katpally et al., 2007; Li et al., 2013). p21 is the viral cell-to-cell movement protein (Rochon and Johnston, 1991) and p20 is a suppressor of RNA silencing (Angel et al., 2011; Hao et al., 2011). p33 and p92 are translated directly from genomic RNA while p41, p21 and p20 are translated from two subgenomic RNAs generated during infection (Johnston and Rochon, 1990, 1995, 1996; Rochon and Johnston, 1991; Sit et al., 1995). As with the p33 proteins of other tombusviruses, CNV p33, or its homolog in *Tomato bushy stunt virus* (TBSV), is an integral membrane protein that is central to the formation of the viral replicase complex. It contains an RNA binding site for specific recruitment of viral RNA into the replication complex, specific domains that promote p33/p33 and p33/p92 interactions and a transmembrane domain for targeting peroxisomes in yeast. P33 interacts with numerous host proteins involved in the assembly, fidelity and regulation of the replicase complex (Nagy, 2011; Nagy et al., 2012; Nagy and Pogany, 2010, 2012; Panavas et al., 2005; Pogany et al., 2005; Rajendran and Nagy, 2003; Serva and Nagy, 2006).

Tombusviruses are known to induce distinctive multivesicular bodies (MVBs) during infection (Martelli et al., 1988). These can derive from peroxisomes as in TBSV and *Cymbidium ringspot virus* (CymRSV) (Jonczyk et al., 2007; McCartney et al., 2005; Navarro et al., 2004; Panavas et al., 2005; Pathak et al., 2008), or from mitochondria as in *Carnation Italian ringspot virus* (CIRV) (Hwang et al., 2008; Weber-Lotfi et al., 2002). However, the origin of the MVBs can depend on the host (Martelli et al., 1988). MVBs derived from peroxisomes undergo a progressive vesiculation of the boundary membrane and contain numerous spherules that are approximately 80–150 nm in diameter which serve as the site of viral RNA replication (Appiano et al., 1983; Martelli et al., 1988; McCartney et al., 2005; Panavas et al., 2005; Pathak et al., 2008). MVBs have been suggested to contain membranous material derived from the endoplasmic reticulum (ER) since ER strands were often seen adjacent to or protruding from MVBs (Martelli et al., 1988). In TBSV infection, p33 traffics from the peroxisome to the ER (McCartney et al., 2005). It has been shown that the ER is the site of replication for TBSV and CymRSV in yeast lacking peroxisomes, demonstrating flexibility in the sites of replication

* Corresponding author at: Agriculture and Agri-Food Canada Pacific Agri-Food Research Centre, 4200 Hwy 97, Summerland, BC, Canada V0H 1Z0.
Tel: +1 250 494 6394; fax: +1 250 494 0755.
E-mail address: Dann.Rochon@agr.gc.ca (D. Rochon).

0042-6822/$ - see front matter © 2014 Published by Elsevier Inc.
http://dx.doi.org/10.1016/j.virol.2013.12.035

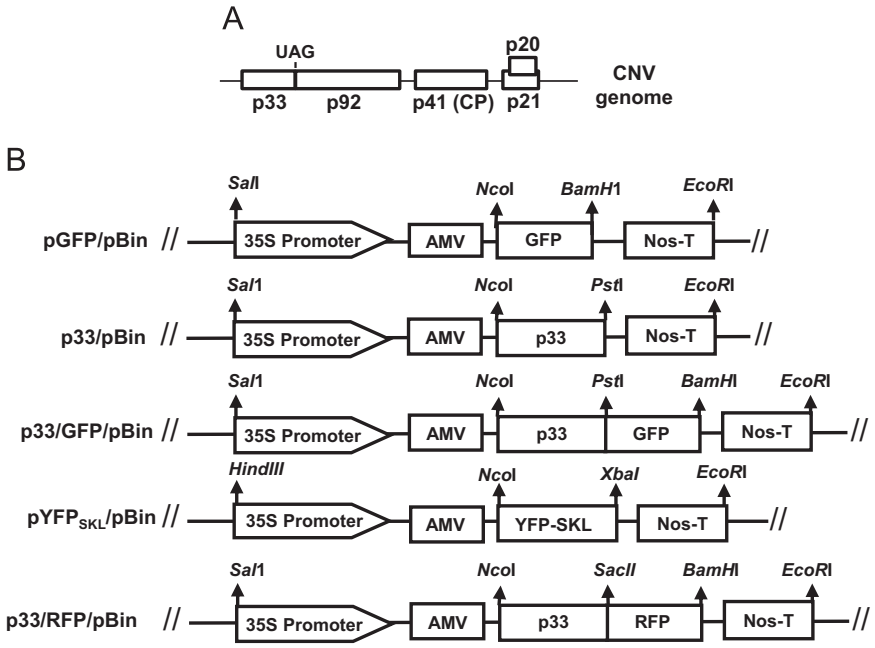

Fig. 1. Diagrammatic representation of constructs used in this study. (A) Boxes in the CNV genome correspond to the five open reading frames which encode the p33 auxiliary replicase protein, the p92 RNA dependent RNA polymerase, the p41 coat protein (CP), the p20 silencing suppressor and the p21 cell-to-cell movement protein. p33 is expressed directly from genomic RNA and p92 is expressed by translational read-through of the p33 amber (UAG) stop codon. (B) Schematic representation of the pBin(+) fusion protein expression constructs used in this study. Clones were constructed as described in Materials and methods section. The desired ORFs were placed downstream of the dual 35S promoter of Cauliflower mosaic virus and the Alfalfa mosaic virus (AMV) translational enhancer. Nos-T corresponds to the nopaline synthase transcription termination site. Restriction enzyme sites used for cloning purposes are shown. pGFP/pBin was previously described (Hui et al., 2010).

of these viruses. In addition, TBSV can replicate efficiently on ER membranes *in vitro* (Jonczyk et al., 2007; Navarro et al., 2004; Xu et al., 2012). Specific sequence elements in p33 have been shown to be involved in peroxisomal or mitochondrial membrane targeting (Burgyan et al., 1996; Hwang et al., 2008; McCartney et al., 2005; Navarro et al., 2004; Panavas et al., 2005; Rubino and Russo, 1998)

CNV p33 has been shown to target peroxisomes in *Saccharomyces cerevisiae* however its targeting site in plants has not been determined. An N-proximal transmembrane domain in CNV p33 is required for peroxisomal targeting in yeast as is a p33:p33/p92 interaction domain (Panavas et al., 2005). Mutations in the interacting domain result in ER rather than peroxisomal targeting of CNV p33.

In this manuscript we show that CNV p33 targets peroxisomes in *N. benthamiana* as well as *N. clevelandii*. The peroxisomes develop into typical MVBs and contain numerous spherules with necks open to the cytoplasm. Some peroxisomes are donut-shaped containing cytoplasm in the center. In addition, we show that the endoplasmic reticulum of CNV infected plants becomes highly remodeled during infection rendering *de novo* production of peroxisomes. Since peroxisomes play an important role in H_2O_2 breakdown we investigated whether CNV infected plants show defects in peroxide metabolism. Using DAB staining, we show that H_2O_2 accumulates in both CNV infected and p33 agroinfiltrated leaves. Since high levels of H_2O_2 are known to induce necrosis in plants, we speculate that infection induced alteration of peroxisomes results in inefficient H_2O_2 breakdown and subsequent necrosis.

Results and discussion

p33 targets peroxisomes in agroinfiltrated plants

To determine the subcellular targeting site of p33, the p33 ORF was fused to the N-terminus of GFP in pBin(+) to produce the construct p33/GFP/pBin (Fig. 1) and this construct was used to agroinfiltrate leaves of *N. benthamiana*. Confocal microscopy showed that at early times post-agroinfiltration (~24 h) cells of leaves contained small, highly mobile fluorescent spherical bodies approximately 0.9–1.6 um in diameter (average = 1.22 um) (Fig. 2A) reminiscent of peroxisomes. GFP fluorescence was found to be predominantly associated with the boundary membrane giving a "haloed" appearance to the peroxisome. In addition, a single punctate foci of brighter fluorescence was often found associated with the boundary membrane (Fig. 2A). At later times post-agroinfiltration (2 days) large aggregates of spheres predominated (Fig. 2B). The peroxisomal nature of the spherical bodies seemed likely since as described above it has previously been shown that CNV p33 associates with peroxisomes in yeast (Panavas et al., 2005) and the p33 proteins of two other tombusviruses are also known to associate with peroxisomes in *N. benthamiana* (McCartney et al., 2005; Navarro et al., 2004). To confirm that the spherical structures associated with CNV p33 correspond to peroxisomes the construct $pYFP_{SKL}$/pBin (Fig. 1) was used in co-agroinfiltration experiments. This construct contains the YFP gene with a C-terminal peroxisomal targeting tripeptide SKL (Gould et al., 1989; Serviene et al., 2005) which results in peroxisomal targeting of YFP. Fig. 2C shows that YFP_{SKL} targets small spherical bodies approximately 1.0–1.8 um in diameter (average = 1.34 um). These bodies were highly mobile as expected (not shown). Note, however, that in this case, the peroxisomal spheres are "filled" since the SKL motif targets YFP to the peroxisomal matrix (Gould et al., 1989; Serviene et al., 2005). It is noted that peroxisomes in $pYFP_{SKL}$/pBin infiltrated plants did not show a high level of aggregation as was observed in p33/GFP/pBin infiltrated leaves indicating that p33/GFP/pBin induces peroxisomal aggregation. This might result from high levels of p33 expression and consequent p33/p33 interaction between peroxisomes since as stated earlier p33 inherently forms dimers. To assess colocalization of p33 and the peroxisomal marker $pYFP_{SKL}$/pBin, p33/GFP/pBin and $pYFP_{SKL}$/pBin were coinfiltrated and leaves were examined by confocal microscopy. It can be seen in Fig. 2E

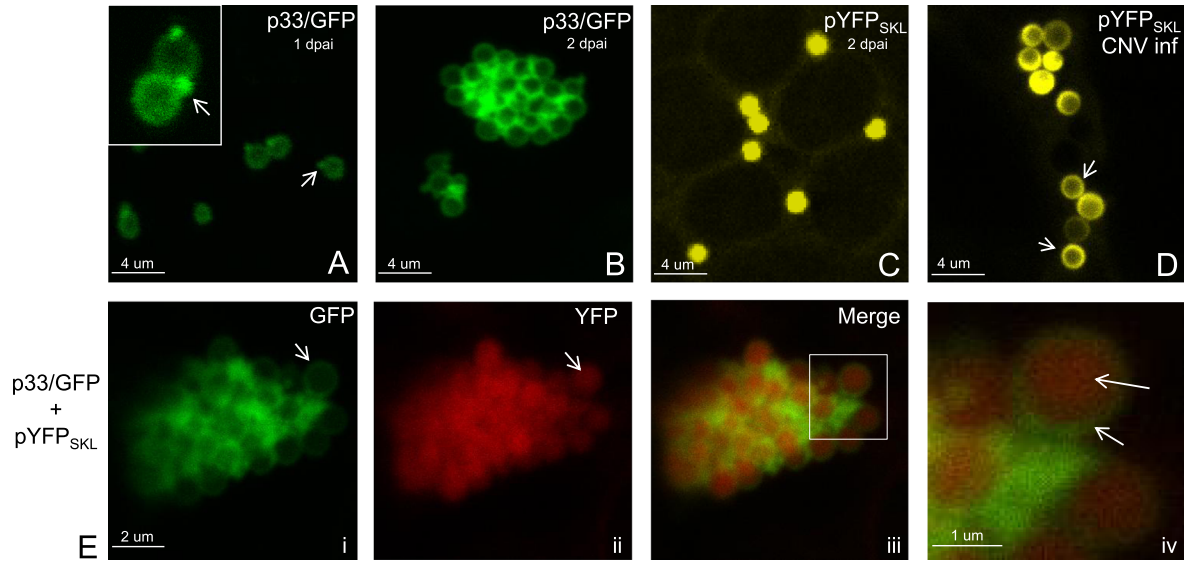

Fig. 2. Confocal microscopy analysis of p33/GFP and pYFP$_{SKL}$ infiltrated *N. benthamiana*. Plants were infiltrated with p33/GFP/pBin or with pYFP$_{SKL}$/pBin and then examined by confocal microscopy after 1 or 2 days as indicated. (D) Plants were infiltrated with pYFP$_{SKL}$ and then inoculated with an infectous CNV cDNA clone pK2/M5 and 3 days later plants were analyzed by confocal microscopy. The arrows in A point to punctate structures often observed on peroxisomes in p33/GFP infected plants. In (A–D), the GFP and YFP channels were allocated false green and yellow colors, respectively. (E) Plants were co-agroinfiltrated with p33/GFP/pBin and pYFP$_{SKL}$/pBin and analyzed by confocal microscopy at 2 days post-infiltration. The arrow in panel i points to the GFP-labeled boundary membrane and in panel ii to the YFP labeled matrix of the peroxisome. The outlined area in the merged image in panel iii is magnified in panel iv to highlight colocalization of the GFP and YFP signals (arrows) In (E), bandwidth mirror settings were adjusted to minimize bleedthrough between channels (see Materials and methods section). Bleedthrough was additionally reduced by using sequential line scanning and DyeFinder software (Leica Microsystems). The GFP and YFP channels were allocated false green and red colors, respectfully and were digitally merged (panel D). Magnification bars are shown.

that the p33/GFP labeled haloed spheres (panel i) overlap with the YFP filled spheres (colored red in panel ii) in the merged image (panel iii, iv). Although there is overlap in the emission spectra of GFP and YFP the distinctive localization of the GFP and YFP signals to the boundary membrane and matrix, respectfully, allows determination of colocalization. In addition, overlap in the emission spectra was minimized by narrowing the detection windows for GFP and YFP to areas of minimal overlap. The images were also scanned sequentially and then processed using Dyefinder software (Leica Microsystems) which removes data where the two spectra overlap. We conclude from these experiments that CNV p33/GFP targets peroxisomes in agroinfiltrated plants.

As noted above, at 36–48 h post-agroinfiltration cells of p33/GFP/pBin infiltrated leaves contained predominantly highly aggregated peroxisomes with most peroxisomes in a cell being present in a single large aggregate (Fig. 2B). This contrasts with what was observed in pYFP$_{SKL}$/pBin infiltrated cells where peroxisomes were usually well-dispersed at 36–48 hpai (Fig. 2C). To assess if peroxisomes in CNV infected cells were aggregated, *N. benthamiana* plants were infiltrated with pYFP$_{SKL}$/pBin followed by immediate inoculation with CNV. At 48 h post-treatment peroxisomes were generally found in aggregates of 3–7 on average (Fig. 2D) and later in infection a high level of aggregation occurred (see below).

An unexpected observation in pYFP$_{SKL}$/pBin infiltrated CNV infected cells was that many peroxisomes appeared to be labeled on the boundary membrane (Fig. 2D) rather than the matrix as observed in uninfected plants (compare with Fig. 2C). As will be described below, peroxisomes become extensively remodeled during CNV infection, often becoming donut-shaped. Labeling of the matrix of such peroxisomes would give the haloed appearance seen in Fig. 2D. It is noted that YFP$_{SKL}$ labeled peroxisomes in CNV infected plants are larger on average (1.9 um) than peroxisomes in uninfected plants infiltrated with p33/GFP/pBin (1.22 um) or pYFP$_{SKL}$ (1.34 um). This is likely a result of the morphological changes that peroxisomes undergo during infection such as membrane proliferation (see below).

Cells of CNV infected leaves contain MVBs derived from peroxisomes

Transmission electron microscopy of CNV infected *N. clevelandii* and *N. benthamiana* plants was conducted to determine if CNV infections induce MVBs as in other tombusvirus infections (see Introduction section). Highly vesiculated bodies ranging in size from approximately 2–7 um are abundant in the cytoplasm of both hosts (Fig. 3). In *N. clevelandii* the bodies often contained catalase crystals (Fig. 3A) as previously noted in other tombusvirus-infected plant cells (Martelli et al., 1988; Martelli and Russo, 1976; McCartney et al., 2005), however, catalase crystals were not found in peroxisomes of CNV infected *N. benthamiana*. The basis for this is unknown but it may relate to the level of infection in examined leaf sections. The presence of catalase in the MVBs of *N. clevelandii* provides evidence for the peroxisomal origin of CNV MVBs in plant cells similar to that observed in yeast cells transfected with CNV (Panavas et al., 2005) and plant cells infected with TBSV (McCartney et al., 2005). Upon close examination of the MVBs, it can be seen that the boundary membrane is highly vesiculated with multiple invaginations of the boundary membrane (see inset in Fig. 3A). These invaginations are similar to the 80–150 nm globose and ovoid structures previously described by others (Martelli et al., 1988; McCartney et al., 2005). These structures resemble spherules that are found in the membranes of organelles used for replication of several plant and animal viruses (Ahlquist, 2006; Laliberte and Sanfacon, 2010). These structural features, in conjunction with studies conducted by Panavas et al. (2005) on CNV replication in yeast, demonstrate that peroxisomes are likely a subcellular site for replication of CNV and that spherules formed in the boundary membrane are likely the compartments in which viral RNA is sequestered for replication.

Fig. 3 shows that MVBs induced by CNV are often donut-shaped such that the central region contains cytoplasm. It has been suggested that these arise *via* invagination of the modified peroxisome (Martelli et al., 1988; Martelli and Russo, 1976). However, the basis for the formation of these distinctive MVBs remains to be determined.

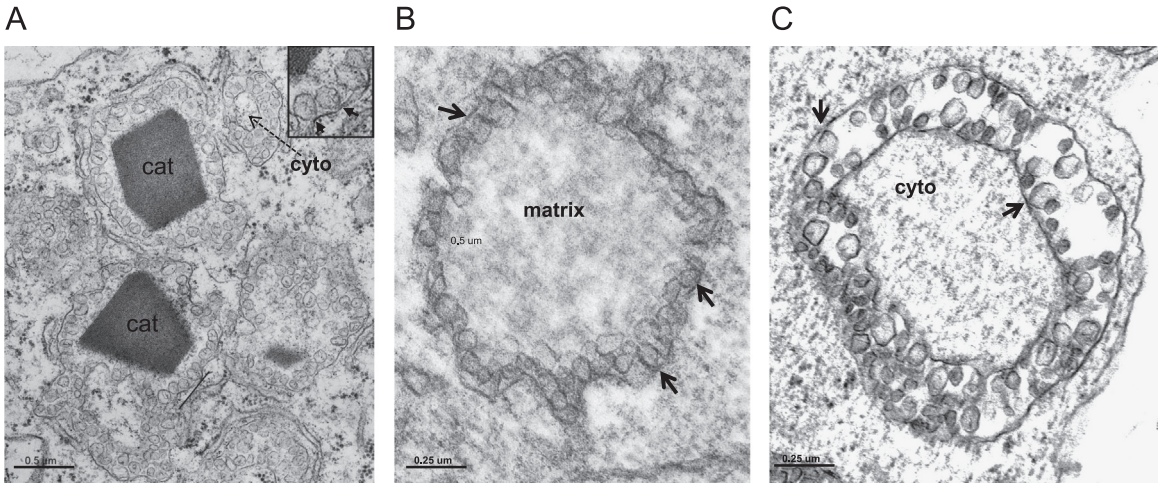

Fig. 3. Transmission electron micrographs of MVBs induced by pK2/M5 in *N. clevelandii* (A) and *N. benthamiana* (B,C). (A) A cluster of MVBs. Note the large catalase (cat) crystals within two of the MVBs. The inset in A shows spherules in more detail and the arrows point to possible necks facing towards the cytoplasm. The dotted arrow in A points to cytoplasmic material present in the interior of a donut-shaped peroxisome. (B) A peroxisome from a pK2/M5 infected *N. benthamiana* plant where the spherules form a single row in association with the boundary membrane and the center corresponds to the peroxisome matrix. (C) As in B except the MVB is donut-shaped with the cytoplasm (cyto) in the peroxisome "interior" and spherules present along the inner and outer facing membranes (see arrows). The matrix would be between the two rows of spherules bounding the inner and outer edge of the "donut"-shaped structure.

The ER of CNV infected plants is extensively remodeled during infection and gives rise to spherical structures resembling peroxisomes and containing peroxisome targeted YFP_{SKL}

As described above, TBSV and CymRSV target ER in yeast cells lacking peroxisomes and peroxisome targeted TBSV p33 is sorted to the peroxisomal subdomain of the ER in infected plant cells. Furthermore, mutations in CNV p33 can result in ER targeting in yeast (Panavas et al., 2005). Our above described studies using p33/GFP/pBin failed to show any association between p33 and the ER. For many viruses the ER becomes highly remodeled to support virus replication (Ahlquist, 2006; den Boon et al., 2010; Laliberte and Sanfacon, 2010). To further assess the possible involvement of ER in CNV replication we infected 16c transgenic plants in which the ER is labeled with GFP, and monitored leaf cells for changes in overall ER structure. Fig. 4A (panels ii, iii) shows that early in infection individual tubules of the ER become thickened and circular structures approximately 2 um in diameter (1.25–3.29 um range; average = 2.0 um) are formed. These were found to be either tethered to the ER or could also be detached and highly mobile (not shown). The circular structures were initially found to exist in small groups of 2–5 (Fig. 4A, panel iii) and then later, by 4 dpi, they were present in large aggregates in the majority of infected cells (Fig. 4A, panel iv). The aggregates were usually perinuclear but were also found at the cell boundary. The thickened circular structures were only very rarely found in uninfected 16c plants and the large aggregates were never observed. Since these structures were similar in size to YFP labeled peroxisomes in CNV infected plants and it is known that peroxisomes arise *de novo* from subdomains of the ER (Hu et al., 2012; Mullen et al., 2001; Tam et al., 2005; Titorenko and Mullen, 2006) we wished to determine if they corresponded to peroxisomes. To assess this, 16c transgenic plants were agroinfiltrated with $pYFP_{SKL}$/pBin followed by immediate inoculation with CNV. As seen in Fig. 4B,C, at 2 dpi, a proportion of the GFP-labeled spherical structures derived from the ER during CNV infection colocalize with YFP_{SKL} labeled peroxisomes. Thus, the peroxisome like structures that arise from the ER during infection appear to indeed represent peroxisomes. It is noted that YFP_{SKL} also labeled peroxisomes that did not coincide with the ER derived structures as would be expected in cases of pre-existing peroxisomes. Our observations raise the intriguing possibility that CNV infection may enhance peroxisome biogenesis from the ER perhaps as a means for increasing sites available for RNA replication.

CNV p33/RFP targets de novo formed peroxisome-like structures in infected plants

To assess whether the *de novo* formed peroxisome-like structures represent sites of CNV replication, 16c plants were agroinfiltrated with p33/RFP/pBin and then immediately inoculated with CNV. Fig. 5A shows that p33/RFP labels peroxisomes in non-transgenic uninfected plants as expected and that as was observed with CNV p33/GFP/pBin agroinfiltrations, labeling occurred on the periphery of the peroxisome, and, as well, peroxisomes were often found in aggregates. Fig. 5 B shows that p33/RFP colocalizes with the peroxisome-like structures induced *de novo* in 16c transgenic plants infected with CNV. Thus, it is possible that these structures may serve as a site for replication of CNV.

Experiments were conducted to determine if p33 alone could result in *de novo* induction of peroxisome-like structures. Examination of p33 agroinfiltrated 16c plants showed an occasional spherical peroxisome-like structure and some disruption of ER membrane organization but these were found infrequently and the large aggregates were never found despite extensive searching. Therefore, either another CNV encoded protein(s) or p33 together with other CNV encoded protein(s) is required for efficient *de novo* induction of peroxisome-like structures.

It is interesting that two possibly distinctive types of peroxisomes appear to exist in tombusvirus infected cells. These peroxisomes may be suited to distinct functions. For example, one type of peroxisome may be involved in the synthesis of RNA for subsequent translation and the other type for subsequent encapsidation. Further research is required to examine these hypotheses. In addition, it is possible that the donut-shaped peroxisomes correspond to peroxisomes that are generated *de novo* from the ER post-infection. However, again, this hypothesis requires further exploration.

TBSV infection induces peroxisome-like structures

As described in the introduction, TBSV replicates in association with peroxisomes in yeast and in plants and can also replicate in association with the ER in the absence of peroxisomes. To expand our observation that CNV induces peroxisome-like structures during infection, we inoculated *N. benthamiana* 16c plants with TBSV and then examined plants by confocal microscopy for

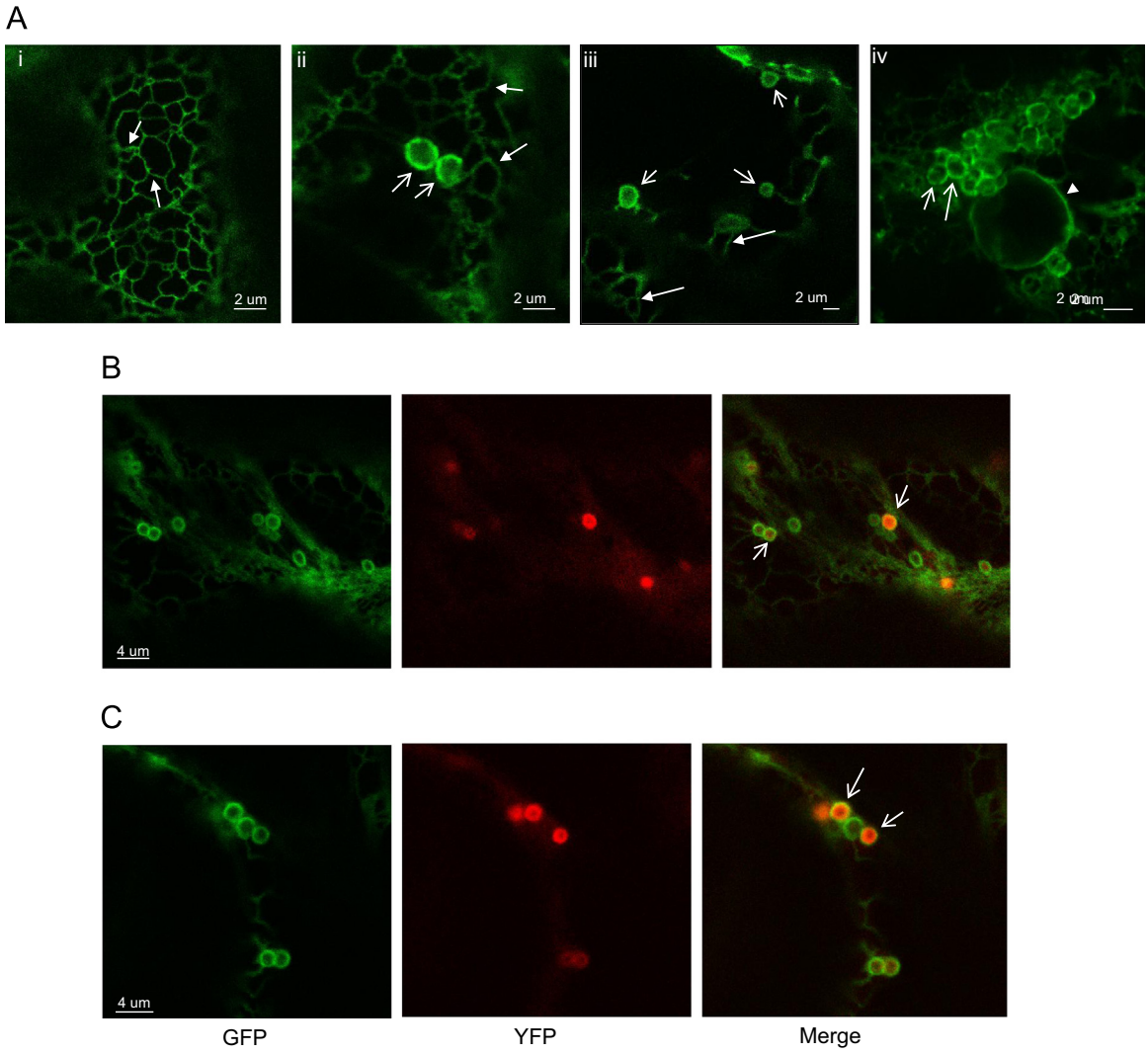

Fig. 4. Confocal microscopy analysis of pK2/M5 infected *N. benthamiana* 16c transgenic plants. (A) Development of circular, thickened areas of ER tubules following pK2/M5 infection (*i*) Mock inoculated 16c plant showing the typical ER network within a cell. pK2/M5 infected 16c plants at 2 dpi (panels ii and iii) and 3 dpi (panel iv). The open arrows point to circular, thickened areas of ER which develop during pK2/M5 infection with panel *iv* showing an aggregate of such structures surrounding the nucleus (indicated by the arrowhead). The closed arrows point to normal ER tubules. Magnification bars are shown. (B,C) Confocal microscopy analysis at 2 dpi of 16c plants infiltrated with $pYFP_{SKL}$ and infected with pK2/M5 showing colocalization of peroxisomes with the circular, thickened areas of the ER that develop during infection. YFP is false colored red. See Fig. 5 for details of microscopy.

evidence of *de novo* peroxisome formation. As can be seen in Fig. 6, peroxisome-like structures similar to those induced by CNV are observed in TBSV infected plants. At 4 dpi these structures are mostly seen in close association with the ER (Fig. 6 A, panel ii) but by 5 dpi numerous large aggregates are observed apparently free from the ER (Fig. 6B, panels i and ii). These observations suggest that TBSV also induces peroxisome-like structures and that this may be true for other tombusviruses that replicate in association with peroxisomes. Further research is required to demonstrate that TBSV replicates in association with the *de novo* generated peroxisome-like structures.

p33 induces necrosis and leaves contain increased levels of peroxide

During the course of the above described experiments we noted that CNV p33 agroinfiltrated plants displayed necrotic symptoms, similar to those observed in CNV-infected plants. We wished to address whether necrosis could result from disabled peroxisomes (MVBs). Catalase is a major constituent of peroxisomes in photosynthetic tissue where it breaks down H_2O_2 that accumulates during photorespiration (Mhamdi et al., 2012; Mhamdi et al., 2010). Mutant *Arabidopsis* or tobacco plants deficient in peroxisomal catalase and grown under high light or long day conditions have been found to accumulate H_2O_2 which induces a hypersensitive response (HR) or renders plants hyper-responsive to pathogen infection (Chamnongpol et al., 1998; Chaouch et al., 2010; Mhamdi et al., 2010, 2012; Mittler et al., 1999). The accumulation of H_2O_2 is believed to be the trigger for HR rather than necrosis being a direct result of H_2O_2 induced damage of cells (Mhamdi et al., 2012; Shapiguzov et al., 2012; Torres et al., 2006). Since peroxisomes are highly modified in CNV infected plants and plants display necrosis (Fig. 7A) we sought to determine if peroxide accumulates in CNV infected plants and in p33/pBin infiltrated leaves as a means to assess if necrotic symptoms result from peroxisome dysfunction. To do this, CNV inoculated leaves and p33/pBin infiltrated leaves at 5 dpi were treated with 3,3 diaminobenzidine-HCl (DAB) which stains leaves brown in areas of H_2O_2 accumulation (Gould et al., 1990; Thordal-Christensen et al., 1997). Fig. 7B shows that CNV infected leaves and p33 infiltrated leaves stain brown whereas uninfected leaves or mock infiltrated leaves do not. Thus leaves of both CNV-infected plants and p33 infiltrated plants accumulate peroxide in regions of infiltration and infection. These results are consistent with the possibility that p33 induces necrosis *via* perturbing

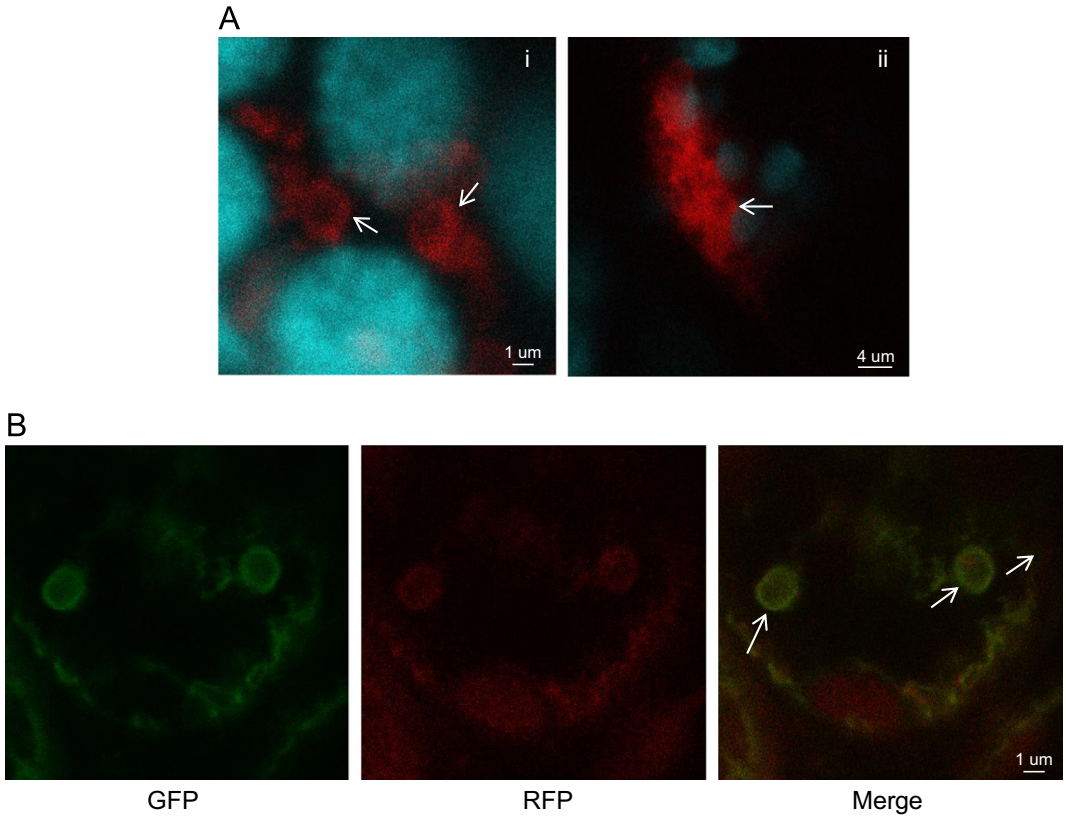

Fig. 5. Confocal microscopy showing co-localization of CNV p33/RFP with CNV-induced peroxisomal-like structures in *N. benthamiana* 16c plants. (A) p33/RFP infiltrated *N. benthamiana* leaves showing peroxisomal localization (arrows). In panel i, peroxisomes are clearly labeled with RFP on the periphery as previously shown with p33/GFP (Fig. 2A). A lower resolution image of an aggregate of peroxisomes is shown in panel ii. Chloroplasts are false colored turquoise. An individual peroxisome is pointed to by the arrow. (B) Colocalization of p33/RFP with ER-derived peroxisomes in CNV-infected 16c plants infiltrated with p33/RFP. 16c plants were agroinfiltrated with p33/RFP and then immediately inoculated with CNV particles. The first panel shows GFP fluorescence, the second panel RFP fluorescence and the third panel is a digitally merged image of the first and second panels. Arrows point to peroxisome-like structures.

the H_2O_2 scavenging function of peroxisomes. However, they do not rule out the possibility that CNV or p33 also induce cytoplasmic apoplastic H_2O_2 accumulation as is often the case in pathogen infection (Torres et al., 2006). Further work is required to link peroxisomal H_2O_2 to symptom induction in CNV infected plants.

In summary, our results show that CNV p33 targets peroxisomes during infection resulting in physiological and elaborate morphological changes in peroxisomes that may lead to the induction of necrosis due to faulty peroxide metabolism. In addition, we show that CNV infection is accompanied by the *de novo* production of peroxisome-like structures that may serve as new sites for CNV replication. While *de novo* production of peroxisomes from the endoplasmic reticulum is a known pathway for new peroxisome formation, less is known regarding factors that induce this process and therefore CNV or TBSV may be a useful tool for studying this phenomenon. Finally, the *de novo* production of new peroxisomes may be a response to elevated levels of peroxide seen in CNV infection, *i.e.*, high levels of peroxide could be a factor that induces *de novo* peroxisome formation as a means for compensating for lowered peroxide metabolizing activity. However, p33 is not sufficient for this response so another viral factor must be involved in enabling the induction of new peroxisomes from the ER.

Materials and methods

Construction of CNV p33/pBin, p33/GFP/pBin, p33/RFP/pBin and pYFP$_{SKL}$/pBin

PCR was used to amplify the ORFs of GFP (see Xiang et al. (2006)) and p33 from the full-length CNV infectious cDNA clone pK2/M5 (Rochon and Johnston, 1991). Primers used for amplification are shown in Table 1. Each primer carried a restriction enzyme recognition site used for subsequent cloning steps. PCR products were digested with the corresponding restriction enzyme, electrophoresed through an agarose gel and gel purified. The purified fragments were then ligated into the corresponding sites of the intermediate vector, pBBI525 (Pang et al., 1992). In the case of p33/GFP/pBin both the p33 and GFP fragments were ligated into pBBI525 simultaneously. Constructs were then digested with SalI and EcoRI and cloned into similarly digested *Agrobacterium tumefaciens* binary vector pBin(+) (Van Engelen et al., 1995). EYFP-peroxi (Clontech; catalog number 6933-1) which contains the EYFP gene fused to the coding sequence for the tripeptide SKL which serves as a peroxisomal targeting signal (Serviene et al., 2005) was used as a template for the production of pYFP$_{SKL}$/pBin. EYFP-peroxi was digested with NcoI (which overlaps the start codon for EYFP) and XbaI (which lies just downstream from the EYFP stop codon) and the gel purified fragment was cloned into similarly digested pBBI525. This resulting construct was then digested with HindIII and EcoRI and cloned into pBin(+). The following procedure was used to construct p33/RFP/pBin. The coding region of RFP (Clontech, catalog number 632479) was amplified by PCR using the forward and reverse primers shown in Table 1 and cloned into an intermediate vector. This construct was digested with SacII and BamHI and ligated into a pBBI525 construct containing p33. The construct was digested with SalI and EcoRI and ligated into similarly digested pBin(+) to yield p33/RFP/pBin. The final structure of the pBin(+) clones are summarized in Fig. 1. pGFP/pBin was previously described (Kopek et al., 2007).

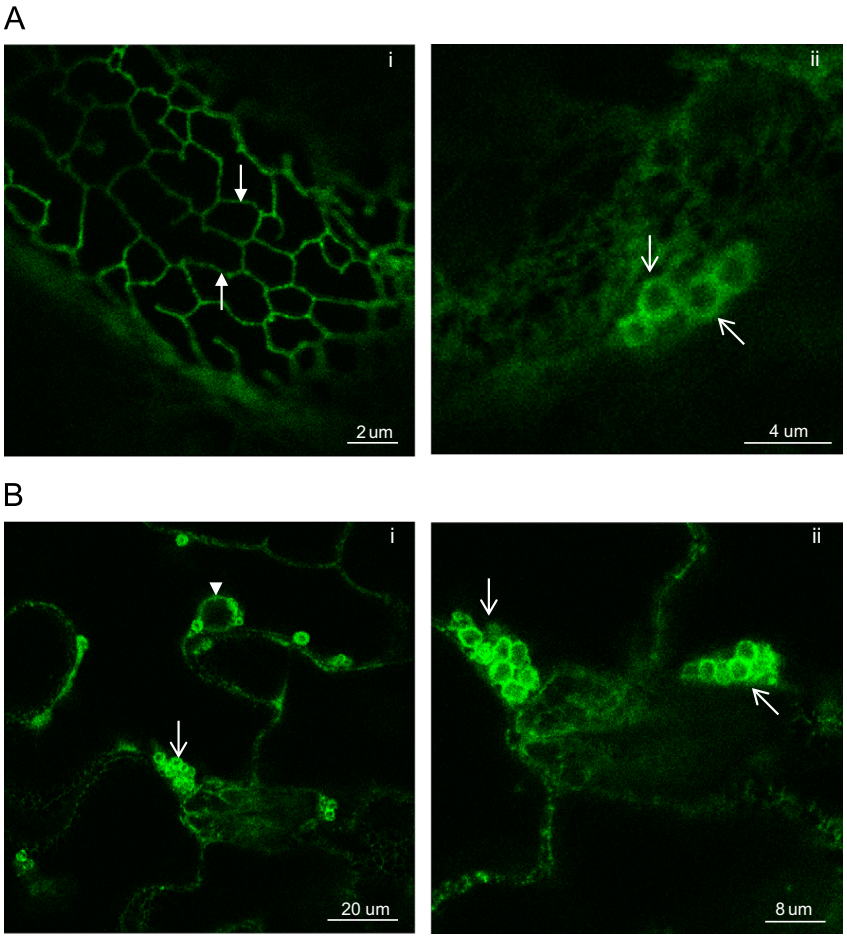

Fig. 6. Confocal microscopy of TBSV infected *N. benthamiana* 16c transgenic plants. (A) TBSV infected 16c plants at 4 dpi (panels i, ii). The closed arrows in panel i point to normal ER tubules. The open arrows in panel ii point to circular, thickened areas of the ER that develop during TBSV infection. (B) TBSV infected 16c plants at 5 dpi. Development of aggregates of peroxisome-like structures (indicated by the arrows) in most cells of an infected leaf area (panel i) and surrounding the nucleus (indicated by the arrowhead in panel i). Panel ii is a magnified view of two clusters of peroxisome-like structures.

Agrobacterium-mediated transient expression

pBin(+) constructs were used to transform *A. tumefaciens* strain GV3101 (Koncz et al., 1986). The agroinfiltration procedure was performed as described previously (Ahlquist, 2006). Transformants were streaked on LB/agar plates containing 50 μg/ml kanamycin and 10 μg/ml rifampicin and incubated at 28 °C overnight. A single colony from the plate was inoculated into 3 ml YEB medium (0.1% yeast extract, 0.5% beef extract, 0.5% peptone, 0.5% sucrose, and 2 mM Mg_2SO_4) containing 50 ug/ml kanamycin and 40 ug/ml rifampin and grown at 28 °C for 48 h with vigorous shaking. One ml of the culture was transferred to 50 ml YEB medium containing the above antibiotics, 10 mM MES, pH 5.6 and 20 μM acetosyringone. After incubation at 28 °C for approximately 20 h with vigorous shaking, bacteria were centrifuged at 4000 g for 6 min at 4 °C. The pellet was resuspended in 50 ml 10 mM MES, pH 5.6 and 10 mM $MgCl_2$, and then 200 μM acetosyringone was added. The bacterial suspension was incubated at room temperature for 3–5 h without shaking. The cultures were used to infiltrate *N. benthamiana* leaves. The $OD_{600\ nm}$ of cells used for agroinfiltration of $pYFP_{SKL}$/pBin was 0.2. For the remaining constructs the $OD_{600\ nm}$ was 1.0 (Gould et al., 1989; Wang et al., 2011).

Inoculation of plants with virus

Macerated leaf tissue in 25 mM potassium phosphate buffer, pH 7.2 infected with the "*Prunus* strain" of TBSV was used for inoculation of *N. benthamiana* 16c plants. This strain was obtained from the Agriculture and Agri-Food Canada plant virus collection.

In vitro transcription and inoculation

In vitro transcription of CNV infectious clone pK2/M5 and subsequent inoculation of plants was conducted as previously described (Rochon and Johnston, 1991). Leaves of 4–6 week old *N. benthamiana* 16c plants, kindly provided by D. Baulcombe, were inoculated with 01–10 μg of CNV per leaf in a 20 μl volume of 10 mM potassium phosphate buffer pH 7.0.

DAB staining

For histochemical determination of hydrogen peroxide, individual leaves from agroinfiltrated *N. benthamiana* plants were immersed in freshly prepared 1,3′-diaminobenzidine (DAB) stain (1 mg/ml DAB in 40 mM HCl, pH 3.0) for 30 min at room temperature (Thordal-Christensen et al., 1997). Tissue was cleared in boiling 95% ethanol for 10 min. A brown precipitate is formed in the leaves in the presence of hydrogen peroxide.

Confocal microscopy

Confocal microscopy was carried out using a Leica TCS SP2-AOBS microscope. The excitation wavelengths used for GFP, YFP and RFP were 488 nm, 514 nm and 543 nm, respectively. The bandwidth

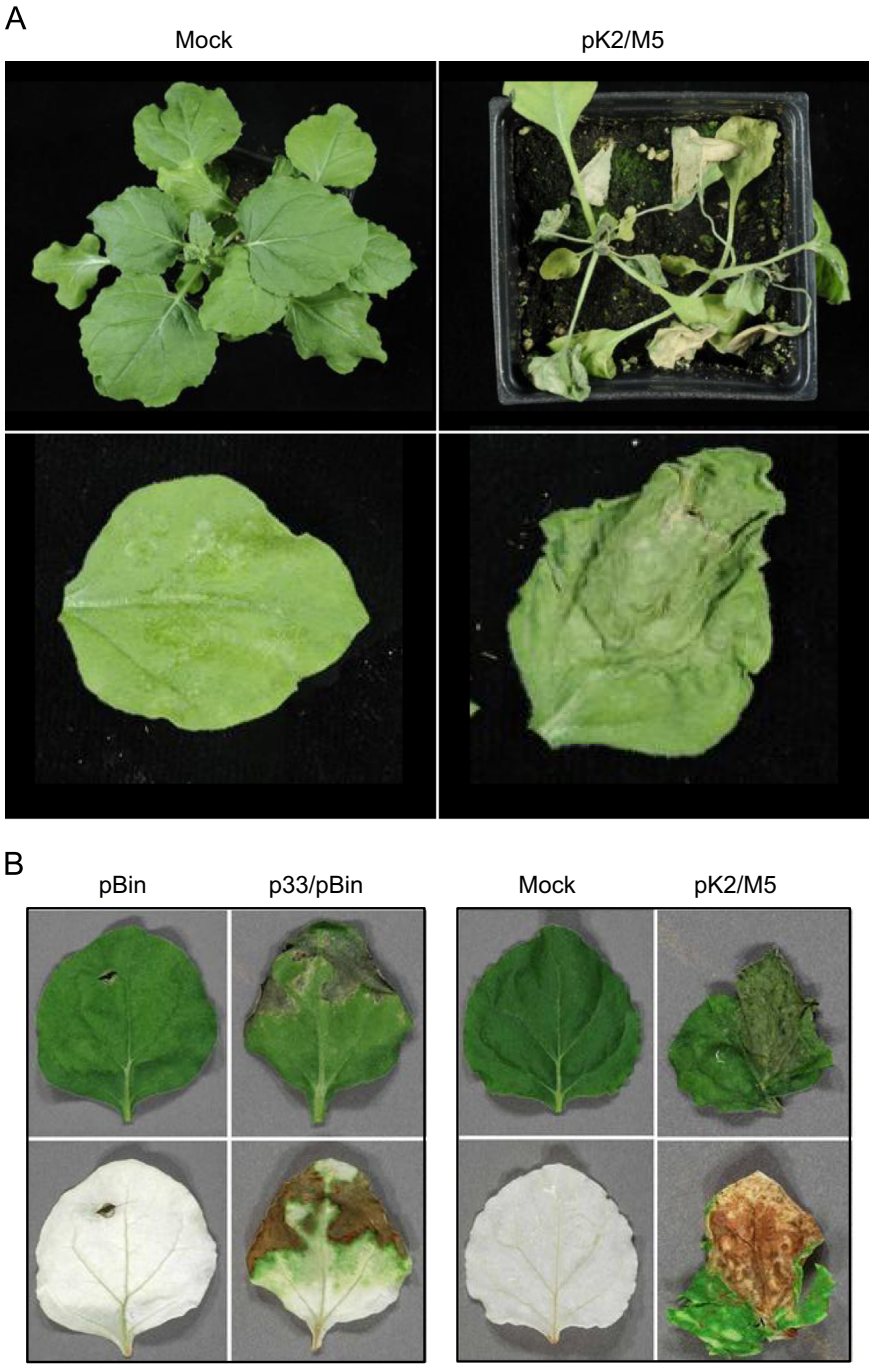

Fig. 7. Infected or agroinfiltrated leaves of pK2/M5 and p33, respectively develop necrosis and accumulate peroxide. (A) Symptoms induced by CNV in *N. benthamiana*. Leaves were either mock inoculated or inoculated with transcripts of pK2/M5 and monitored for symptoms. Individual inoculated leaves were photographed at 6 dpi and whole plants at 9 dpi. Note that leaves show extensive necrosis. (B) DAB staining of p33/pBin agroinfiltrated or CNV infected leaves for detection of increased peroxide. *N. benthamiana* leaves were agroinfiltrated with vector only (pBin) or p33/pBin or were mock infected or infected with pK2/M5 as indicated. Agroinfiltrated or infected leaves at 5 dpi were stained with 1,3 diaminobenzidine (DAB) to assess hydrogen peroxide accumulation. DAB staining was followed by ethanol treatment which bleaches unstained areas of the leaf. The upper panels show leaves prior to DAB staining and the lower panel following DAB staining. The brown precipitate observed in p33/pBin agroinfiltrated and pK2/M5 infected leaves is indicative of peroxide accumulation.

mirror settings for discriminating between GFP and YFP were 493–518 nm (GFP) and 585–612 nm (EYFP). Bleedthrough between channels was reduced by using sequential line scanning and by using DyeFinder software (Leica Microsystems) to further remove bleedthrough. The two channels were allocated false green (GFP) and red (YFP) colors. When RFP was used in conjunction with GFP, the GFP bandwidth mirror settings were narrowed so that bleedthrough into the RFP channel was not evident and *vice versa*. The degree of narrowing depended on the relative strengths of the GFP and RFP signals for a given image.

Transmission electron microscopy

Tissue samples from symptomatic areas of CNV infected *N. clevelandii* or *N. benthamiana* were fixed in 2.5% glutaraldehyde in fixation buffer (0.1 M sodium cacodylate, pH 7.2) for 3 h at room temperature. Samples were first placed in a vacuum for 1 h to facilitate infiltration of the fixative. Samples were washed 3 times for 10 min each in fixation buffer and then post-fixed in 1% osmium tetroxide in fixation buffer. Samples were washed in

Table 1
Oligonucleotides used for cloning pBin constructs shown in Fig. 1.

Primer name[a]	Primer sequence[b]
Nco1_p33_F	5′CAAGACC**ATG**GTGTGGCCTAAGAAAG3′
Pst1_p33_R	5′AAGCCCTGCAGTTT*CA*CACCAAGGGAC3′
Pst1_GFP_F	5′ATATACTGCAGGTGAGCAAGGGCG3′
BamH1_GFP_R	5′TATTAGGATCC*TTA*CTTGTACAGCTCGTA3′
SacII_RFP_F	5′AACCGCGG**ATG**GACAACACCGAGGACGTCATCAAGG3′
BamH1_RFP_R	5′AAGGATCC*TTA*CTGGGAGCCGGAGTGGCGGGCCTCG3′

[a] The primer name indicates the ORF that it was used to amplify, the restriction enzyme site that was introduced and whether the primer is a forward (F) or reverse (R) primer.
[b] The underlined region shows the restriction enzyme site used for cloning purposes (name of restriction enzyme is in the name of the primer, left column of table) and the italicized letters correspond to an introduced stop codon. Start codons are in bold type.

deionized water 3 times for 10 min each and then dehydrated through a graded ethanol series up to 100%. Embedding was in Spurr's Epon. Light gold sections (60–90 nm) were stained in lead citrate and uranyl acetate and viewed with a JEOL 100CX transmission electron microscope (TEM) operated at 60 kV.

Acknowledgments

We thank Michael Weis for expert assistance in confocal microscopy and Dr. R. Mullen for providing TBSV p33 antibody. K.G and S.B.A. were supported by NSERC Discovery Grants 10R82367 and 10R82.

References

Ahlquist, P., 2006. Parallels among positive-strand RNA viruses, reverse-transcribing viruses and double-stranded RNA viruses. Nat. Rev. Microbiol. 4, 371–382.
Angel, C.A., Hsieh, Y.C., Schoelz, J.E., 2011. Comparative analysis of the capacity of tombusvirus P22 and P19 proteins to function as avirulence determinants in *Nicotiana* species. Mol. Plant Microbe Interact. 24, 91–99.
Appiano, A., Bassi, M., D'Agostino, G, 1983. Cytochemical and autoradiographic observations on tomato bushy stunt virus-induced multivesicular bodies. Ultramicroscopy 12, 162.
Burgyan, J., Rubino, L., Russo, M., 1996. The 5′-terminal region of a tombusvirus genome determines the origin of multivesicular bodies. J. Gen. Virol. 77 (Pt 8), 1967–1974.
Chamnongpol, S., Willekens, H., Moeder, W., Langebartels, C., Sandermann Jr., H., Van Montagu, M., Inze, D., Van Camp, W., 1998. Defense activation and enhanced pathogen tolerance induced by H_2O_2 in transgenic tobacco. Proc. Natl. Acad. Sci. U.S.A 95, 5818–5823.
Chaouch, S., Queval, G., Vanderauwera, S., Mhamdi, A., Vandorpe, M., Langlois-Meurinne, M., Van Breusegem, F., Saindrenan, P., Noctor, G., 2010. Peroxisomal hydrogen peroxide is coupled to biotic defense responses by isochorismate synthase1 in a daylength-related manner. Plant Physiol. 153, 1692–1705.
den Boon, J.A., Diaz, A., Ahlquist, P., 2010. Cytoplasmic viral replication complexes. Cell Host Microbe 8, 77–85.
Gould, S.J., Keller, G.A., Hosken, N., Wilkinson, J., Subramani, S., 1989. A conserved tripeptide sorts proteins to peroxisomes. J. Cell Biol. 108, 1657–1664.
Gould, S.J., Krisans, S., Keller, G.A., Subramani, S., 1990. Antibodies directed against the peroxisomal targeting signal of firefly luciferase recognize multiple mammalian peroxisomal proteins. J. Cell Biol. 110, 27–34.
Hao, X., Lu, A., Sokal, N., Bhagwat, B., Leung, E., Mao, R., Reade, R., Wu, Y., Rochon, D., Xiang, Y., 2011. Cucumber necrosis virus p20 is a viral suppressor of RNA silencing. Virus Res. 155, 423–432.
Hu, J., Baker, A., Bartel, B., Linka, N., Mullen, R.T., Reumann, S., Zolman, B.K., 2012. Plant peroxisomes: biogenesis and function. Plant Cell 24, 2279–2303.
Hui, E., Xiang, Y., Rochon, D., 2010. Distinct regions at the N-terminus of the Cucumber necrosis virus coat protein target chloroplasts and mitochondria. Virus Res 153, 8–19.
Hwang, Y.T., McCartney, A.W., Gidda, S.K., Mullen, R.T., 2008. Localization of the Carnation Italian ringspot virus replication protein p36 to the mitochondrial outer membrane is mediated by an internal targeting signal and the TOM complex. BMC Cell Biol. 9, 54.
Johnston, J.C., Rochon, D.M., 1990. Translation of cucumber necrosis virus RNA in vitro. J. Gen. Virol. 71 (Pt 10), 2233–2241.
Johnston, J.C., Rochon, D.M., 1995. Deletion analysis of the promoter for the cucumber necrosis virus 0.9-kb subgenomic RNA. Virology 214, 100–109.
Johnston, J.C., Rochon, D.M., 1996. Both codon context and leader length contribute to efficient expression of two overlapping open reading frames of a cucumber necrosis virus bifunctional subgenomic mRNA. Virology 221, 232–239.
Jonczyk, M., Pathak, K.B., Sharma, M., Nagy, P.D., 2007. Exploiting alternative subcellular location for replication: tombusvirus replication switches to the endoplasmic reticulum in the absence of peroxisomes. Virology 362, 320–330.
Katpally, U., Kakani, K., Reade, R., Dryden, K., Rochon, D., Smith, T.J., 2007. Structures of $T=1$ and $T=3$ particles of cucumber necrosis virus: evidence of internal scaffolding. J. Mol. Biol. 365, 502–512.
Koncz, C., Schell, J., 1986. The promoter of Ti-DNA gene controls the tissue-specific expression of chimaeric genes by a novel type of *Agrobacterium* binary vector. Mol. Gen. Genet. 204, 383–396.
Kopek, B.G., Perkins, G., Miller, D.J., Ellisman, M.H., Ahlquist, P., 2007. Three-dimensional analysis of a viral RNA replication complex reveals a virus-induced mini-organelle. PLoS Biol. 5, e220.
Laliberte, J.F., Sanfacon, H., 2010. Cellular remodeling during plant virus infection. Annu. Rev. Phytopathol. 48, 69–91.
Li, M., Kakani, K., Katpally, U., Johnson, S., Rochon, D., Smith, T.J., 2013. Atomic structure of cucumber necrosis virus and the role of the capsid in vector transmission. J. Virol. 87, 12166–12175.
Martelli, G.P., Gallitelli, D., Russo, M., 1988. Tombusviruses. In: Koenig, R. (Ed.), The Plant Viruses: Polyhedral Virions with Monopartite RNA Genomes. Plenum Press, New York(pp. 13–72).
Martelli, G.P., Russo, M., 1976. Unusual cytoplasmic inclusions induced by watermelon mosaic virus. Virology 72, 352–362.
McCartney, A.W., Greenwood, J.S., Fabian, M.R., White, K.A., Mullen, R.T., 2005. Localization of the tomato bushy stunt virus replication protein p33 reveals a peroxisome-to-endoplasmic reticulum sorting pathway. Plant Cell 17, 3513–3531.
Mhamdi, A., Noctor, G., Baker, A., 2012. Plant catalases: peroxisomal redox guardians. Arch. Biochem. Biophys. 525, 181–194.
Mhamdi, A., Queval, G., Chaouch, S., Vanderauwera, S., Van Breusegem, F., Noctor, G., 2010. Catalase function in plants: a focus on Arabidopsis mutants as stress-mimic models. J. Exp. Bot. 61, 4197–4220.
Mittler, R., Herr, E.H., Orvar, B.L., van Camp, W., Willekens, H., Inze, D., Ellis, B.E., 1999. Transgenic tobacco plants with reduced capability to detoxify reactive oxygen intermediates are hyperresponsive to pathogen infection. Proc. Natl. Acad. Sci. U.S.A 96, 14165–14170.
Mullen, R.T., Lisenbee, C.S., Flynn, C.R., Trelease, R.N., 2001. Stable and transient expression of chimeric peroxisomal membrane proteins induces an independent "zippering" of peroxisomes and an endoplasmic reticulum subdomain. Planta 213, 849–863.
Nagy, P.D., 2011. The roles of host factors in tombusvirus RNA recombination. Adv. Virus Res. 81, 63–84.
Nagy, P.D., Barajas, D., Pogany, J., 2012. Host factors with regulatory roles in tombusvirus replication. Curr. Opin. Virol. 2, 691–698.
Nagy, P.D., Pogany, J., 2010. Global genomics and proteomics approaches to identify host factors as targets to induce resistance against Tomato bushy stunt virus. Adv. Virus Res. 76, 123–177.
Nagy, P.D., Pogany, J., 2012. The dependence of viral RNA replication on co-opted host factors. Nat. Rev. Microbiol. 10, 137–149.
Navarro, B., Rubino, L., Russo, M., 2004. Expression of the Cymbidium ringspot virus 33-kilodalton protein in *Saccharomyces cerevisiae* and molecular dissection of the peroxisomal targeting signal. J. Virol. 78, 4744–4752.
Panavas, T., Hawkins, C.M., Panaviene, Z., Nagy, P.D., 2005. The role of the p33:p33/p92 interaction domain in RNA replication and intracellular localization of p33 and p92 proteins of Cucumber necrosis tombusvirus. Virology 338, 81–95.
Pang, S.-Z., Nagpala, P., Wang, M., Slightom, J.L., Gonsalves, D., 1992. Resistance to heterologous isolates of tomato spotted wilt virus in transgenic tobacco expressing its nucleocapsid protein gene. *Phytopathology* 82, 1223–1229.
Pathak, K.B., Sasvari, Z., Nagy, P.D., 2008. The host Pex19p plays a role in peroxisomal localization of tombusvirus replication proteins. Virology 379, 294–305.
Pogany, J., White, K.A., Nagy, P.D., 2005. Specific binding of tombusvirus replication protein p33 to an internal replication element in the viral RNA is essential for replication. J. Virol. 79, 4859–4869.
Rajendran, K.S., Nagy, P.D., 2003. Characterization of the RNA-binding domains in the replicase proteins of tomato bushy stunt virus. J. Virol. 77, 9244–9258.
Rochon, D.M., Johnston, J.C., 1991. Infectious transcripts from cloned cucumber necrosis virus cDNA: evidence for a bifunctional subgenomic mRNA. Virology 181, 656–665.
Rochon, D.M., Tremaine, J.H., 1989. Complete nucleotide sequence of the cucumber necrosis virus genome. Virology 169, 251–259.
Rubino, L., Russo, M., 1998. Membrane targeting sequences in tombusvirus infections. Virology 252, 431–437.
Serva, S., Nagy, P.D., 2006. Proteomics analysis of the tombusvirus replicase: Hsp70 molecular chaperone is associated with the replicase and enhances viral RNA replication. J. Virol. 80, 2162–2169.
Serviene, E., Shapka, N., Cheng, C.P., Panavas, T., Phuangrat, B., Baker, J., Nagy, P.D., 2005. Genome-wide screen identifies host genes affecting viral RNA recombination. Proc. Natl. Acad. Sci. U.S.A 102, 10545–10550.
Shapiguzov, A., Vainonen, J.P., Wrzaczek, M., Kangasjarvi, J., 2012. ROS-talk - how the apoplast, the chloroplast, and the nucleus get the message through. Front. Plant Sci. 3, 292.

Sit, T.L., Johnston, J.C., ter Borg, M.G., Frison, E., McLean, M.A., Rochon, D., 1995. Mutational analysis of the cucumber necrosis virus coat protein gene. Virology 206, 38–48.

Tam, Y.Y., Fagarasanu, A., Fagarasanu, M., Rachubinski, R.A., 2005. Pex3p initiates the formation of a preperoxisomal compartment from a subdomain of the endoplasmic reticulum in *Saccharomyces cerevisiae*. J. Biol. Chem. 280, 34933–34939.

Thordal-Christensen, H., Brandt, J., Cho, B.H., Gregersen, P.L., Rasmussen, S.K., Smedegaard-Petersen, V., Collinge, D.B., 1997. cDNA cloning and characterization of two barley peroxidase transcripts induced differentially by the powdery mildew fungus *Erysiphe graminis*. Physiol. Mol. Plant Pathol. 40, 395–409.

Titorenko, V.I., Mullen, R.T., 2006. Peroxisome biogenesis: the peroxisomal endomembrane system and the role of the ER. J Cell Biol 174, 11–17.

Torres, M.A., Jones, J.D., Dangl, J.L., 2006. Reactive oxygen species signaling in response to pathogens. Plant Physiol. 141, 373–378.

Van Engele, F.A., Molthoff, J.W., Conner, A.J., Nap, J.P., Pereira, A., Stiekema, W.J., 1995. pBINPLUS: an improved plant transformation vector based on pBIN19. Transgenic Res 4, 288–290.

Wang, X., Diaz, A., Hao, L., Gancarz, B., den Boon, J.A., Ahlquist, P., 2011. Intersection of the multivesicular body pathway and lipid homeostasis in RNA replication by a positive-strand RNA virus. J. Virol. 85, 5494–5503.

Weber-Lotfi, F., Dietrich, A., Russo, M., Rubino, L., 2002. Mitochondrial targeting and membrane anchoring of a viral replicase in plant and yeast cells. J. Virol. 76, 10485–10496.

Xiang, Y., Kakani, K., Reade, R., Hui, E., Rochon, D., 2006. A 38-amino-acid sequence encompassing the arm domain of the cucumber necrosis virus coat protein functions as a chloroplast transit peptide in infected plants. J. Virol 80, 7952–7964.

Xu, K., Huang, T.S., Nagy, P.D., 2012. Authentic in vitro replication of two tombusviruses in isolated mitochondrial and endoplasmic reticulum membranes. J. Virol. 86, 12779–12794.